# Accelerated discovery and mapping of block copolymer phase diagrams

Elizabeth A. Murphy, <sup>1,2,3</sup> Stephen J. Skala, <sup>1,3,4</sup> Dimagi Kottage, <sup>1,2</sup> Phillip A. Kohl, <sup>1,3</sup> Youli Li, <sup>1,3</sup> Cheng Zhang, <sup>1,5</sup> Craig J. Hawker, <sup>1,2,3,4,\*</sup> and Christopher M. Bates, <sup>1,2,3,4,6,†</sup>

<sup>1</sup>Materials Research Laboratory, University of California, Santa Barbara, California 93106, USA

<sup>2</sup>Department of Chemistry & Biochemistry, University of California, Santa Barbara, California 93106, USA

<sup>3</sup>BioPACIFIC Materials Innovation Platform, University of California, Santa Barbara, California 93106, USA

<sup>4</sup>Materials Department, University of California, Santa Barbara, California 93106, USA

<sup>5</sup>Australian Institute for Bioengineering and Nanotechnology and Centre for Advanced Imaging University of Queensland, Brisbane,

Queensland 4072, Australia

<sup>6</sup>Department of Chemical Engineering, University of California, Santa Barbara, California 93106, USA



(Received 26 August 2023; accepted 20 October 2023; published 25 January 2024)

Block copolymers are widely used in many applications due to their spontaneous self-assembly into a variety of nanoscale morphologies. However, a grand challenge in navigating this diverse and ever-growing array of possible structures is the accelerated discovery, design, and implementation of materials. Here, we report a versatile and efficient strategy to accelerate materials discovery by rapidly building expansive, high-quality, and detailed block copolymer libraries through a combination of controlled polymerization and chromatographic separation. To illustrate the potential of this approach, a family of 16 parent diblock copolymers was synthesized and separated, leading to over 300 distinct and well-defined samples at the multigram scale. The resulting materials span a wide range of compositions with exceptional resolution in volume fraction and domain spacing that allows for the impact of monomer design on polymer self-assembly to be elucidated. Phase behavior that can be gleaned from these libraries includes the precise location of order-order boundaries and the identification of morphologies with extremely narrow windows of stability. This user-friendly, scalable, and automated approach to discovery significantly increases the availability of well-defined block copolymers with tailored molecular weights, molar-mass dispersities, compositions, and segregation strengths, accelerating the study of structure-property relationships in advanced soft materials.

DOI: 10.1103/PhysRevMaterials.8.015602

### I. INTRODUCTION

Block copolymers are a common class of materials that self-assemble into a variety of well-ordered nanoscale morphologies, including sphere phases, hexagonally packed cylinders, double gyroid networks, and lamellae [1]. The distinct ability of block copolymers to spontaneously selfassemble into well-defined nanostructures underpins their versatility, enabling applications in diverse areas such as advanced separation membranes [2,3], thermoplastic elastomers [4,5], photonic crystals [6,7], microelectronics [8,9], and drug delivery [10]. Key to these and other applications is the ability to tune self-assembly behavior through synthetic handles including block chemistry, composition, and molecular weight using controlled polymerization techniques that have undergone significant advances over the past few decades [11]. However, minor changes in monomer structure and pairing can yield dramatic, often unexpected differences

Published by the American Physical Society under the terms of the Creative Commons Attribution 4.0 International license. Further distribution of this work must maintain attribution to the author(s) and the published article's title, journal citation, and DOI.

in self-assembly [12,13]. This fact exemplifies a key challenge associated with navigating the vast design space of (multi)block copolymers and underscores the potential advantages of developing an accelerated approach to materials discovery [14–16].

Traditionally, constructing even incomplete phase diagrams requires time-consuming and costly iterative synthesis to vary block copolymer parameters such as composition and molecular weight [17]. The repetitive synthesis of each block copolymer is also complicated by slight variations in reaction conditions and/or purification that lead to undesired (but unavoidable) differences among samples. As a result, currently available approaches to generate libraries of related block copolymers hinder a fundamental understanding of experimental phase behavior. For example, Bates et al. examined the equilibrium phase behavior of polyisoprene-polystyrene diblock copolymers through a limited library of 10 samples spanning a polyisoprene volume fraction (f) from 0.24 to 0.82 [18]. Each diblock copolymer required synthesis, purification, and characterization over two steps and represents only a single data point on the phase diagram. To accelerate this discovery process, Davidock et al. [19] and Ren et al. [20,21] postfunctionalized a series of 1,4-polyisopreneb-poly(ethylethylene) diblock copolymers through selective difluorocarbene modification to systematically vary the Flory-Huggins interaction parameter  $(\chi)$ . While successful,

<sup>\*</sup>hawker@mrl.ucsb.edu

<sup>†</sup>cbates@ucsb.edu

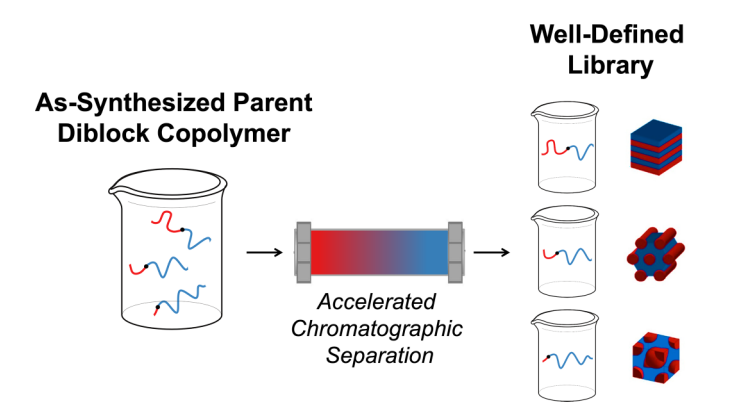


FIG. 1. Automated chromatographic fractionation of an assynthesized parent diblock copolymer leads to a well-defined library of samples enabling the accelerated development of detailed phase diagrams.

this functionalization process also results in drastic changes in volume fraction, domain spacing, and statistical segment length (b), leading to distinct phase behavior for each modified polymer.

Motivated by the grand challenge to accelerate materials design and discovery, here, we report a versatile and scalable method for the efficient mapping of phase diagrams across related families of diblock copolymers [22]. In this paper, we build upon our previous efforts to rapidly prepare well-defined block copolymer libraries and discrete oligomers through chromatographic separation (see Fig. 1) [12,23–43]. In marked contrast to expensive and time-consuming iterative discovery methods, we report the preparation of over 300 purified and well-defined diblock copolymers from the synthesis and separation of only 16 parent samples. The utility of this approach is demonstrated through the facile generation of four comprehensive phase diagrams across a monomer family of semifluorinated acrylates spanning a range of molecular weights with enhanced resolution that allows the influence of monomer design to be examined in detail. The broad exploration of phase space is further enhanced by the ability to precisely tune volume fractions and achieve domain spacings with angstrom-level resolution within individual phase regions.

## II. METHODS

Block copolymers were synthesized using sequential photoinitiated atom transfer radical polymerization (ATRP) [44]. The photomediated ATRP light source (UV:  $\lambda_{max}\approx 360$  nm) was a commercial nail curing lamp (Thermal Spa) equipped with  $3\times 16$  W bulbs. Solution state  $^1H$  nuclear magnetic resonance (NMR) spectra were recorded on a Varian 600 MHz spectrometer. Chemical shifts ( $\delta$ ) are reported in ppm relative to residual protiosolvent in CDCl $_3$  (7.26 ppm). NMR measurements were performed with samples concentrations of 10--20~mg/mL. Size-exclusion chromatography (SEC) was conducted on a Waters Alliance HPLC System, 2690 Separation Module using chloroform with 0.25% triethylamine as the eluent with a flow rate of 0.35 mL/min. Refractive index

traces from a Waters 2410 differential refractometer detector were used for estimates of the molar mass and dispersity relative to linear polystyrene standards with a chloroform mobile phase. Differential scanning calorimetry (DSC) was performed using a TA Instruments DSC Q2000 from -90 to  $55\,^{\circ}$ C at a heating/cooling rate of  $10\,^{\circ}$ C/min using 3–5 mg of sample in a sealed Tzero aluminum pan.

Automated flash chromatography was performed on a Biotage Selekt unit installed with an external evaporative light scattering detector, using Biotage Sfär cartridge series (50 g/100 g) eluted with suitable hexanes/ethyl acetate solvent gradients. All chromatographic solvents were American Chemical Society (ACS) grade or better and used without further purification. In fractionation experiments, the mass recovery was taken as the ratio of the collected mass to the injected mass. Separation conditions were screened using thin-layer chromatography.

Small-angle x-ray scattering measurements were collected on a custom-built high brilliance laboratory beamline for small and wide angle x-ray scattering (SAXS/WAXS) at the BioPACIFIC Materials Innovation Platform at UC Santa Barbara. The instrument is constructed using a high brightness liquid metal jet x-ray source (D2+ 70 kV from Excillum), a low background scatterless slit beam collimation system developed in house, and a 4 megapixel hybrid photon counting area detector (Eiger2 R 4M from Dectris) housed inside a 3-m-long vacuum vessel. The combination of the high brightness source and a large area detector results in  $>10\times$ reduction in data collection times compared with standard labbased SAXS/WAXS instruments, enabling high-throughput nanostructural characterization of a wide range of samples. Two-dimensional data were reduced to a one-dimensional form of intensity (arbitrary units) as a function of the magnitude of the wave vector  $q = |\mathbf{q}| = 4\pi \sin(\theta/2)/\lambda$ , where  $\lambda$ is the x-ray wavelength and  $\theta$  is the scattering angle. Samples consisted of 5–10 mg of bulk polymer pressed within a metal washer backed with Kapton tape annealed at 115 °C for 10 min, then 70 °C for 12 h under vacuum (200 mTorr).

### III. RESULTS AND DISCUSSION

A family of AB diblock copolymers was designed in this study to expand the scope of monomers used in previous reports based on the following considerations: (1) compatibility with controlled polymerization for preparing low-dispersity materials [45], (2) a synthesis platform that enables systematic tuning of the semifluorinated sidechain, (3) the presence of different semifluorinated sidechains in one block leading to a large and variable interaction parameter  $(\chi)$  and the formation of well-defined nanostructures at a low degree of polymerization (N) [46-49], and (4) having thermal transitions below room temperature to facilitate facile processing under mild conditions. The versatility of photoinitiated ATRP enabled the efficient and controlled synthesis of AB diblock copolymers with a tunable degree of fluorination based on A = poly(dodecyl acrylate) (D) and B = fluorinated acrylate (F) monomers. Four classes of AB diblock copolymers with increasing degrees of fluorination were synthesized via sequential photo-ATRP starting from ethyl  $\alpha$ -bromoisobutyrate initiator: poly(dodecyl acrylate)-b-poly(2-fluoroethyl acrylate) (D-1F), poly(dodecyl acrylate)-b-poly(2,2,3,3,3-pentafluoropropyl acrylate) (D-5F),poly(dodecyl acrylate)-b-poly(1H,1H,2H,2Hnonafluorohexyl acrylate) (D-9F), and poly(dodecyl acrylate)-b-poly(2,2,3,3,4,4,5,5,6,6,7,7-dodecafluoroheptyl acrylate) (D-12F). To facilitate comparisons among these materials, a single poly(dodecyl acrylate) starting block was synthesized under photo-ATRP conditions using an aliphatic tertiary amine ligand (Me<sub>6</sub> Tren) and low concentrations of copper (II) bromide (CuBr<sub>2</sub>) with UV irradiation (360 nm light) in a cosolvent mixture of toluene and 2,2,2-trifluoroethanol (TFE) (Scheme S2 in the Supplemental Material [44]). This synthetic strategy resulted in high chain-end fidelity and low molar-mass dispersity, allowing for complete characterization and storage prior to subsequent chain extension reactions. The precursor poly(dodecyl acrylate) homopolymer was chain-extended with the aforementioned semifluorinated acrylate monomers having various degrees of fluorination ranging from 1 to 12 fluorine atoms with all reactions performed under similar conditions using either TFE or 2-trifluoromethyl-2-propanol (TFMP) as a cosolvent. The latter solubilizes all reagents while preventing minor amounts of transesterification side reactions observed with TFE and long-chain fluoroalkyl monomers [45]. The efficiency of photo-ATRP over a broad monomer scope coupled with high chain-end fidelity enabled the preparation of well-defined families of related AB diblock copolymers in excellent yields. Note that the sample nomenclature reflects the block chemistry (D-1F, D-5F, D-9F, or D-12F, see Scheme 1), places  $f_F \times 100$  after the dash (e.g., D-12F-68%), and uses angle brackets \(\lambda\). to denote characteristics of the parent diblock copolymers before fractionation.

The characterization of all AB diblock copolymers was facilitated through unique <sup>1</sup>H NMR resonances for each block. Distinct poly(dodecyl acrylate) resonances were observed at  $\sim$ 4 ppm (resonance b) and  $\sim$ 0.9 ppm (resonance c), as shown in Fig. 2, whereas the 1F block has diagnostic resonances at  $\sim$ 4.3 ppm (resonance d) and  $\sim$ 4.5 ppm (resonance e), 5F at  $\sim$ 4.5 ppm (resonance f), 9F at  $\sim$ 4.3 ppm (resonance g), and 12F at  $\sim$ 4.5 ppm (resonance h) and  $\sim$ 6.0 ppm (resonance i). Significantly, a common unique resonance for the initiator fragment (resonance a) allowed for end-group analysis and an accurate calculation of the experimental molecular weight and volume fraction of each block, which was determined to be in good agreement with the theoretical molecular weights. These results, combined with the observation of expected shifts to lower retention times after chain-extension by SEC, illustrate the high degree of control over polymer formation (Fig. 3). Note that the highly fluorinated diblock copolymers exhibit a chromatogram with a negative differential refractive index upon chain extension due to a lower refractive index than the eluent (chloroform).

To demonstrate the versatility of automated chromatography combined with controlled polymerization for the preparation of diversified polymer libraries, a series of fluorinated diblock copolymers was prepared on multigram scale. As-synthesized diblock copolymers were then dissolved in dichloromethane and loaded directly onto a commercially available (50 g) silica gel column. Suitable elution conditions

SCHEME 1. Synthesis of D-1F, D-5F, D-9F, and D-12F diblock copolymers through sequential photoinitiated atom-transfer radical polymerization.

were identified through a series of thin-layer chromatography (TLC) experiments based on solvent mixtures from 100% hexanes to 100% ethyl acetate (Fig. S25 in the Supplemental Material [44]). More polar diblock copolymers with a single fluorine on the side chain, D-1F, were shown to elute between 60 and 80 vol. % ethyl acetate in hexanes, whereas relatively nonpolar and hydrophobic D-5F, D-9F, and D-12F materials eluted between 20 and 40 vol. % ethyl acetate in hexanes. It is noteworthy that materials with varying degrees of fluorination, polarity, molecular weight, and composition could all be fractionated on multigram scales with excellent mass recoveries (>80%), highlighting the utility of this chromatographic approach to afford polymer libraries irrespective of as-synthesized material properties.

Characterization of the resulting libraries by integration of unique  $^1H$  NMR resonances for each block revealed that the individual fractions spanned a broad compositional window as summarized in Fig. 4. To illustrate the power of this strategy, as-synthesized D-12F-39%—which exhibited a narrow and symmetric molecular weight distribution with  $\langle D \rangle = 1.10$  (Table S18 in the Supplemental Material [44])—was efficiently fractionated into a broad range of diblock copolymers with  $f_{\rm F}=0.06-0.61$  and  $M_{\rm n,F}=0.5-10\,{\rm kDa}$  [Fig. 4(d)].

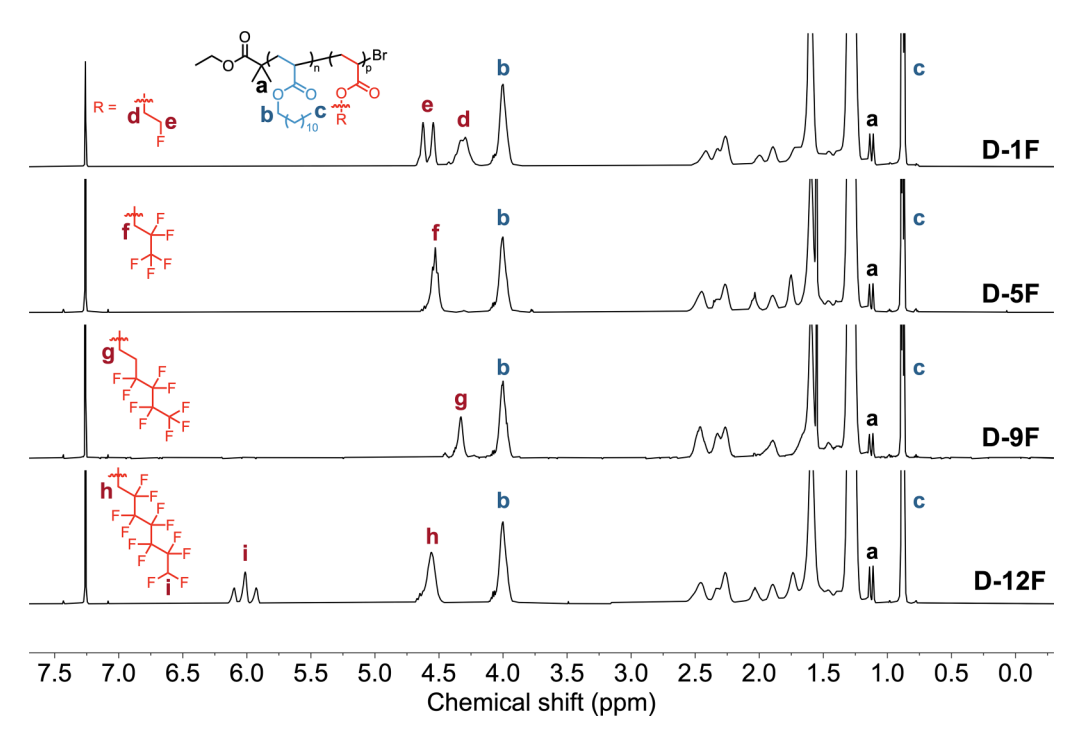


FIG. 2. <sup>1</sup>H nuclear magnetic resonance (NMR) spectra of D-1F, D-5F, D-9F, and D-12F diblock copolymers. The initiator fragment, poly(dodecyl acrylate) block, and fluorinated blocks all exhibit unique resonances.

Notably, the volume fraction of the fluorinated block gradually increases with the solvent gradient as the poly(dodecyl acrylate) volume fraction decreases. This high degree of fractionation was observed for all diblock copolymers regardless of parent chemistry, polarity, composition, and molecular weight. In each case, the separation mechanism is likely driven by selective adsorption of the semifluorinated block as evidenced by <sup>1</sup>H NMR end-group analysis, where the molecular weight of the fluorinated block  $(M_{n,F})$  gradually increases with the solvent gradient in stark contrast to the molecular weight  $(M_{n,D})$  of poly(dodecyl acrylate) that remains relatively constant (Table S21 in the Supplemental Material [44]). An important feature of automated chromatography is the ability to accurately and reproducibly control the solvent gradient (Fig. S26 and Table S2 in the Supplemental Material [44]), enabling the generation of fractionated samples with finely spaced compositions ( $\Delta f \sim 1\%$ ), which would otherwise be difficult to access by iterative synthesis alone. In addition, chromatography allows for the detection and removal of small amounts of homopolymer impurity (<2-3%) generated during synthesis but which is typically difficult to identify and discard; such homopolymer impurities have been shown to significantly impact the self-assembly of block copolymers [50–52].

To demonstrate the utility of automated chromatography in accelerating a systematic mapping of phase behavior, 12 additional diblock copolymers were prepared with strategically selected molecular weights and compositions (Tables S3, S8, S14, and S18 in the Supplemental Material [44]). Parent materials of each copolymer pair were designed to each occupy a unique position in their corresponding phase diagrams with significant differences in composition  $\langle f_{\rm F} \rangle = 0.14$ –0.68 and overall molecular weight  $\langle M_{\rm n} \rangle = 5$ –25 kDa but comparable

dispersities  $\langle D \rangle = 1.05$ –1.15. Notably, the synthesis and separation of these 16 materials gave rise to >320 purified and well-defined diblock copolymers. Specifically, the successful fractionation of four D-1F as-synthesized diblock copolymers produced 78 well-defined fractionated samples, five D-5F parents generated 104 samples, three D-9F parents gave rise to 54 samples, and four D-12F parents produced 87 well-defined samples. The preparation of a diblock copolymer library with this breadth of molecular weights and compositions through iterative synthesis alone would be overwhelming and time consuming, involving multiple synthesis, purification, and intermediate characterization steps for each individual sample. In contrast, this chromatographic technique is complete within  $\sim$ 1 h

The extensive library of high-purity diblock copolymers was then used to comprehensively map the self-assembly behavior of these related sidechain fluorinated derivatives (Fig. 5). SAXS measurements were used to create phase diagrams with an enhanced degree of compositional resolution, plotted as overall molecular weight  $(M_n)$  of the block copolymer in kDa as a function of the fluorinated-block volume fraction  $f_F$ . Due to the breadth of samples generated from a few strategically synthesized diblock copolymers, a wide range of volume fractions ( $f_F = 0.02-0.80$ ) was analyzed to identify a variety of well-defined phases that follow the sequence disordered (DIS)  $\rightarrow$  body-centered cubic spheres (BCC) → hexagonally packed cylinders (HEX)  $\rightarrow$  double gyroid (GYR)  $\rightarrow$  lamellae (LAM) with increasing  $f_F$ . Remarkably, chromatographic separation enabled the entire LAM region for both D-5F and D-12F to be traversed, with even well-defined inverse D-12F HEX structures consisting of a poly(dodecafluoroheptyl acrylate) matrix decorated with poly(dodecyl acrylate) cylinders being observed at

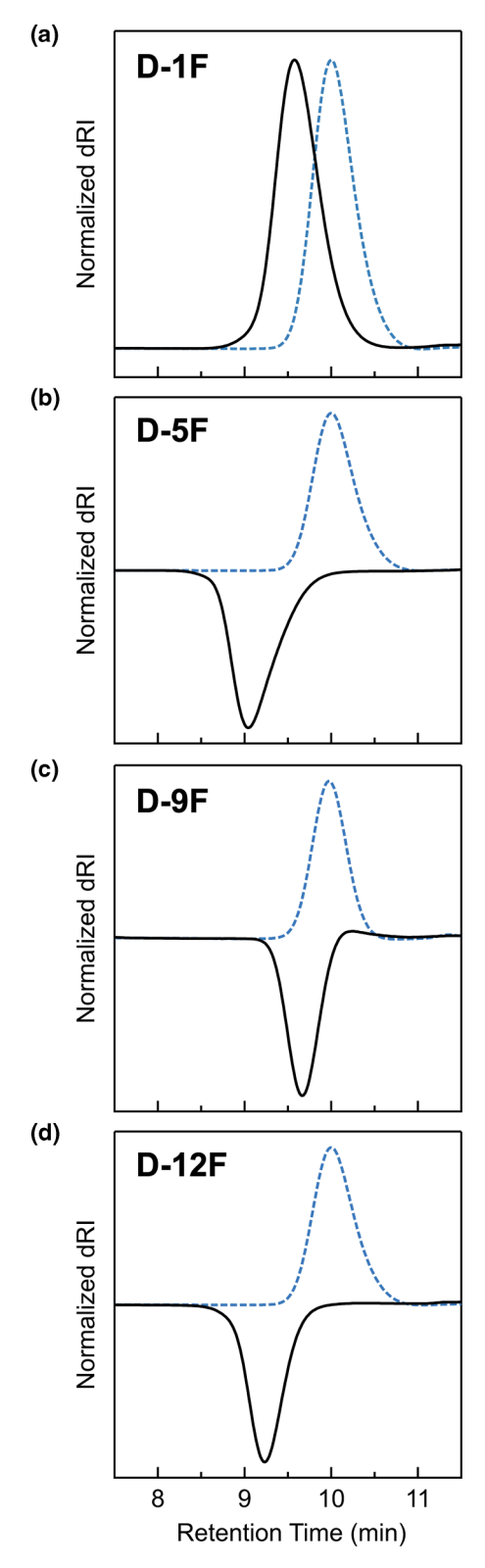


FIG. 3. Size-exclusion chromatograms (normalized differential refractive index signal, dRI) of representative D-1F, D-5F, D-9F, and D-12F diblock copolymers prepared by sequential photomediated atom transfer radical polymerization (ATRP). Dodecyl acrylate was polymerized first (dashed blue lines) followed by growth of the fluorinated block (solid black lines). Note that the dodecyl acrylate homopolymer and D-1F diblock have positive dn/dc values in chloroform whereas D-5F, D-9F, and D-12F have negative dn/dc values.

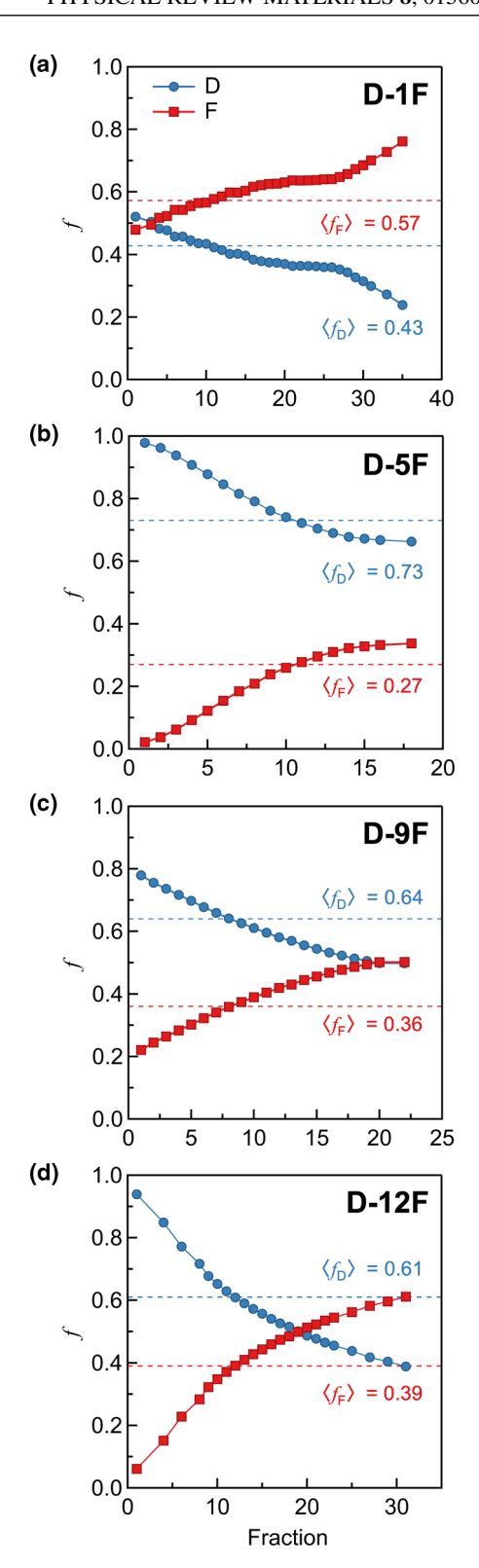


FIG. 4. Chromatographic separation of parent diblock copolymers affords large libraries of fractionated samples. The F-block volume fraction systematically increases in all cases, regardless of starting parent chemistry and composition. Representative fractionations of D-1F, D-5F, D-9F, and D-12F diblock copolymers under similar separation conditions. Fraction represents the polymer recovered in numbered test tubes collected in 22 mL increments. Dashed lines represent the average composition  $\langle f \rangle$  of the starting parent diblock copolymer before fractionation.

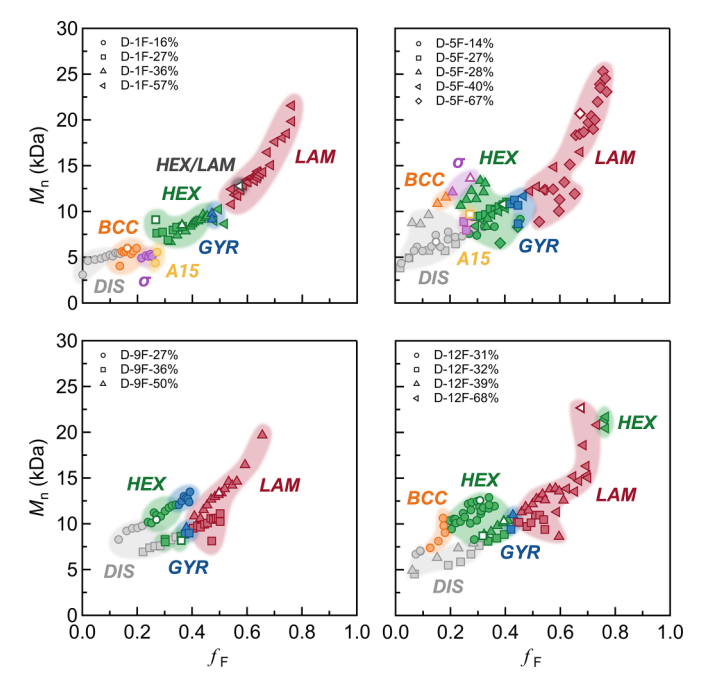


FIG. 5. A library of >320 well-ordered diblock copolymers derived from the synthesis and separation of only 16 samples enabled the preparation of four comprehensive phase diagrams with a high degree of compositional resolution. As-synthesized parent materials are depicted with an open symbol. Fractionated diblock copolymers are depicted with the same shape as their respective parent material but filled. Color indicates the morphology as determined by small-angle x-ray scattering.

 $f_{\rm F} = 0.76 - 0.77$ . The power of this separation strategy in preparing comprehensive and detailed phase diagrams from a limited number of as-synthesized samples is further highlighted by the ability to rapidly and precisely identify morphologies with extremely narrow windows of stability  $(\sim 1\% f_{\rm F})$ , such as GYR, which was consistently found in all four phase diagrams. This finding is important, as phases with small windows of stability are likely to be missed or may be difficult to target synthetically through traditional discovery approaches. In addition, automated chromatography directly addresses the challenges associated with homopolymer impurities and reproducibly preparing high-quality morphologies with narrow regions of phase stability, which classically limits applications such as high-performance separation membranes [53–55], drug delivery, and lithography. The significant control over block copolymer composition and molecular weight afforded by automated chromatography also allows precise order-order boundaries ( $\sim 1\% f_{\rm F}$ ) to be determined. Comparing libraries across increasing degrees of fluorination showed that the HEX, GYR, and LAM phase boundaries shift toward lower  $f_{\rm F}$  at comparable molecular weights.

The rapid generation of samples using this approach allowed us to systematically examine the influence of conformational asymmetry  $(\varepsilon)$  on diblock copolymer phase diagrams by modulating the sidechain length while maintaining a sufficiently high  $\chi$  from the presence of fluorine atoms. For D-1F diblock copolymers, a significant region of  $\sigma$  stability was observed in the range  $f_F = 0.21$ –0.25 and

A15 in the range  $f_F = 0.26-0.27$ , all with long-range order (Fig. S27 in the Supplemental Material [44]), suggesting  $\varepsilon = b_{1F}/b_D > 1$ . Clear order-order boundaries from DIS  $\rightarrow$  $BCC \rightarrow \sigma \rightarrow A15 \rightarrow HEX \rightarrow GYR \rightarrow LAM$  were identified as expected in conformationally asymmetric materials [56–59]. As the sidechain length and degree of fluorination increase further, D-5F formed  $\sigma$  over a narrower region with no complex sphere phases detected for D-9F and D-12F diblock copolymers because the statistical segments lengths of the blocks should be more closely matched. Furthermore, a growing body of experimental and simulation work has shown the formation of complex sphere phases at large conformational asymmetry is sensitive to molar mass dispersity and homopolymer impurities generated by the statistical nature of the polymerization process [60-62]. For example, Lynd and Hillmyer [63] have demonstrated increased molar-mass dispersity in one block leads to phase changes like that of increasing the statistical segment length of the block. Similarly, Dorfman [64] and Cheong et al. [65] have shown that Frank-Kasper phases can be stabilized through the introduction of a minority-block homopolymer. The accelerated discovery and purification process described here is critical to provide reproducible insights into the effect of monomer design and conformational asymmetry in well-defined systems without resorting to discrete oligomer chemistry that is arduous and difficult to scale [66-68]. Notably, a single A15 sample was identified for the parent material D-5F-27% with  $\langle D \rangle = 1.04$ , in contrast to a very similar fractionated sample with the same  $f_{\rm F}$  and overall molecular weight but modestly reduced dispersity of D = 1.02, which formed  $\sigma$  (Fig. S43 in the Supplemental Material [44]). This result underscores the level of sensitivity to dispersity and purity in self-assembly that automated chromatography can reveal when analyzing block copolymer phase diagrams (Fig. S44 in the Supplemental Material [44]). Fractionation was also shown to improve long-range order in complex sphere phases, where purified  $\sigma$ samples exhibited a greater number of reflections compared with the corresponding parent D-5F-28% that also formed it (Fig. S33 in the Supplemental Material [44]).

As shown above, the combination of automated chromatography and controlled polymerization allows for mapping phase space with a high degree of compositional resolution. Due to the significant control over block copolymer fractionation through the use of automation, domain spacings (d) within single-phase regions can be precisely and systematically tuned as a function of  $f_F$  (Fig. 6). For example, the fractionation of parent material D-12F-31% exhibiting a HEX morphology (p6mm) afforded 24 well-defined HEX fractions with improved long-range order in the range  $f_{\rm F} =$ 0.20–0.34 (Table S18 in the Supplemental Material [44]). This range of fractionated samples spans domain spacings over 50 Å for the {10} family of planes  $[d_{10} = 2\pi/q^*]$ , where  $q^*$ is the magnitude of the scattering wave vector at the (10) Bragg peak] with fine separation (< 2 Å) between data points [Fig. 6(a)]. This systematic modulation of domain spacing is clearly observed from the SAXS patterns, where the position of  $q^*$  progressively shifts toward lower q with increasing  $f_F$ and molecular weight of the block copolymer [Fig. 6(b)]. Remarkably, SAXS patterns also reveal changes in the cylinder size of the fluorinated block, as its cylindrical form factor

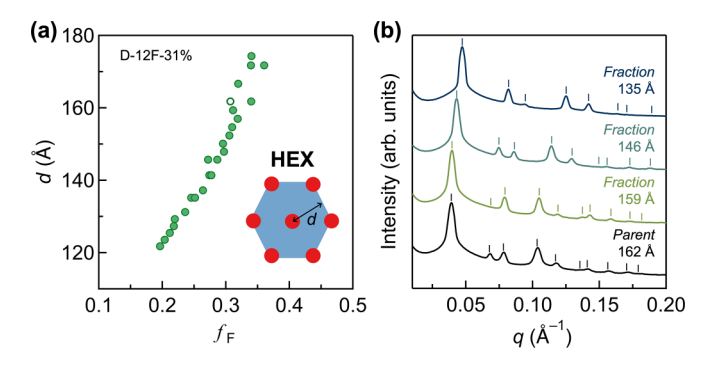


FIG. 6. Automated chromatographic fractionation of block copolymers allows for a high degree of precision in fractionated samples. (a) Domain spacing of hexagonally packed cylinders systematically increases with  $f_{\rm F}$  after fractionation. Note the assynthesized parent material has a domain spacing 9.4 Å larger than the analogous fraction. As-synthesized parent material is depicted with an open symbol. Fractionated diblock copolymers are depicted with filled symbols. (b) Selected small-angle x-ray scattering (SAXS) profiles of a parent diblock copolymer D-12F-31% and fractions derived therefrom. All SAXS experiments were conducted at room temperature. Vertical lines represent theoretical reflections of the given crystal system as calculated based on the experimental  $q^*$ . The position of  $q^*$  progressively shifts toward lower q and larger domain spacings with increasing  $f_{\rm F}$ .

can be seen systematically modulating the intensity of Bragg reflections for fractionated samples. As shown in Fig. 6(b), unlike the parent sample, the (11) peak is completely suppressed for the fractionated sample of similar domain spacing and corresponds to a cylinder diameter of 112 Å for the fluorinated block. As the domain spacing decreases, the minimum in the form factor shifts to higher q (cylinder diameter of ~96 and 79 Å for the 146 and 135 Å fractionated samples, respectively), resulting in the  $\sqrt{3}q^*$  and  $\sqrt{4}q^*$  reflections concomitantly appearing and disappearing. It is important to note that this level of detail would be a significant challenge with iterative synthesis strategies due to inherent limitations caused by the statistical nature of the polymerization process and variations among different synthetic samples. Notably, the parent material D-12F-31% has a domain spacing 9.4 Å larger than the corresponding fractionated sample with the same  $f_{\rm F} = 0.31$ . This result is attributed to the increased purity and reduced dispersity of the fractionated sample and aligns with previous experimental and theoretical work demonstrating that domain spacing increases with dispersity [63,69–71].

The versatility of our chromatographic separation strategy provides the ability to finely tune the domain spacing for other morphologies as well. To highlight this reproducible and broadly applicable strategy, 16 well-defined LAM fractions were shown to systematically traverse domain spacings from  $132 \text{ Å} \rightarrow 203 \text{ Å}$  with increasing  $f_F$  based on the fractionation of only one as-synthesized parent material, D-5F-67% (Table S13 in the Supplemental Material [44]). For this library, the magnitude of the interplanar spacing d was calculated by  $d = 2\pi/q^*$  (Fig. 7). As observed for the series of HEX fractions discussed above, improved sample purity affords reduced domain spacings at equivalent  $f_F$  compared with as-synthesized parent diblock copolymers. For this series, the parent material

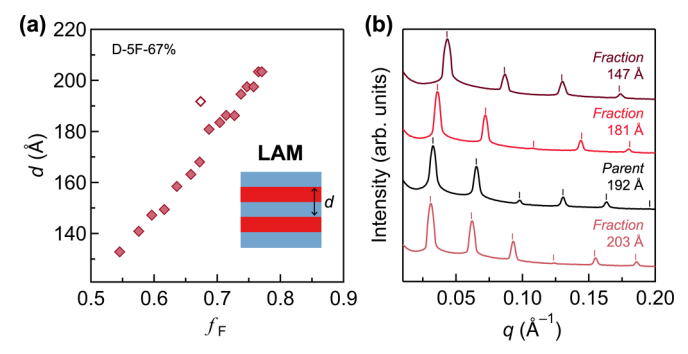


FIG. 7. (a) The domain spacing of fractionated diblock copolymers that form lamellae systematically increases with  $f_{\rm F}$ . Assynthesized parent material has a domain spacing 24 Å larger than the corresponding fractionated material with  $f_{\rm F}=0.67$ . Assynthesized parent material is depicted with an open symbol. Fractionated diblock copolymers are depicted with filled symbols. (b) Selected small-angle x-ray scattering (SAXS) profiles of a parent diblock copolymer D-5F-67% and fractions derived therefrom. All SAXS experiments were conducted at room temperature. Vertical lines represent theoretical reflections of the given crystal system as calculated based on the experimental  $q^*$ . The position of  $q^*$  progressively shifts toward lower q and larger domain spacings with increasing  $f_{\rm F}$ .

D-5F-67% exhibits a 24 Å larger domain spacing than the corresponding fractionated sample with  $f_{\rm F}=0.67$ . The power of this approach to systematically tune the domain spacing of LAM morphologies should be beneficial in applications that demand careful control over microstructure, including sub-10 nm domains for directed self-assembly and polymer photonic crystals where large domain sizes (>100 nm) are necessary to interact with visible light [72–75]. By significantly increasing the availability of well-defined diblock copolymer libraries with precise control over both composition and structure, subtle changes in nanoscale structure are readily achieved.

## IV. CONCLUSIONS

In summary, we have described a versatile and efficient strategy for the accelerated mapping and discovery of phase diagrams in diblock copolymer systems. By combining controlled polymerization with automated flash chromatography, >300 purified and well-defined diblock copolymers were obtained via the synthesis of only 16 parent samples. The power of this method was highlighted through the rapid generation of comprehensive phase diagrams with exceptional compositional and structural resolution, enabling the reproducible investigation of how monomer design and sidechain functionality impact self-assembly. This automated approach provides access to well-defined polymer libraries under user-friendly conditions with a degree of precision that is challenging to achieve using traditional iterative synthesis. The increased synthetic availability of large block copolymer libraries should facilitate synergistic collaborations across a range of soft matter research areas in the future, for example, to promote data-driven discovery.

All curated data are available in this paper or the Supplemental Material [44]. The data that support the findings of this paper are openly available in Dryad [76].

### **ACKNOWLEDGMENTS**

This paper was primarily supported by the National Science Foundation (NSF) Materials Research Science and Engineering Center (MRSEC) at UC Santa Barbara (NSF No. DMR-2308708, IRG-1) and the BioPACIFIC Materials Innovation Platform of the NSF under Award No. DMR-1933487 (C.M.B., C.J.H., equipment and characterization). This paper made use of shared facilities of the MRSEC at UC Santa Barbara: NSF No. DMR-2308708. The UC Santa Barbara

MRSEC is a member of the Materials Research Facilities Network [77]. E.A.M. and S.J.S. gratefully acknowledge the NSF Graduate Research Fellowship Program under Grant No. 2139319. C.Z. acknowledges support from the National Health and Medical Research Council for an Early Career Fellowship (No. APP1157440) and the Australian Research Council for his Discovery Early Career Researcher Award fellowship (No. DE230101105).

The manuscript was written by E.A.M., C.J.H., and C.M.B.. Experiments were designed by E.A.M., S.J.S., D.K., P.A.K., Y.L., C.Z., C.J.H., and C.M.B. and performed by E.A.M., S.J.S., D.K., and P.A.K.. All authors have given approval to the final version of the manuscript.

The authors declare no competing financial interest.

- [1] F. S. Bates and G. H. Fredrickson, Block copolymers-designer soft materials, Phys. Today **52**(2), 32 (1999).
- [2] S. Pereira Nunes, Block copolymer membranes for aqueous solution application, Macromolecules 49, 2905 (2016).
- [3] Y. Zhang, N. E. Almodovar-Arbelo, J. L. Weidman, D. S. Corti, B. W. Boudouris, and W. A. Phillip, Fit-for-purpose block polymer membranes molecularly engineered for water treatment, npj Clean Water 1, 2 (2018).
- [4] N. A. Lynd, F. T. Oyerokun, D. L. O'Donoghue, D. L. Handlin, and G. H. Fredrickson, Design of soft and strong thermoplastic elastomers based on nonlinear block copolymer architectures using self-consistent-field theory, Macromolecules 43, 3479 (2010).
- [5] J. R. Blankenship, A. E. Levi, D. J. Goldfeld, J. L. Self, N. Alizadeh, D. Chen, G. H. Fredrickson, and C. M. Bates, Asymmetric miktoarm star polymers as polyester thermoplastic elastomers, Macromolecules 55, 4929 (2022).
- [6] M. Poutanen, G. Guidetti, T. I. Gröschel, O. V. Borisov, S. Vignolini, O. Ikkala, and A. H. Gröschel, Block copolymer micelles for photonic fluids and crystals, ACS Nano 12, 3149 (2018).
- [7] S. Liu, Y. Yang, L. Zhang, J. Xu, and J. Zhu, Recent progress in responsive photonic crystals of block copolymers, J. Mater. Chem. C 8, 16633 (2020).
- [8] C. M. Bates, M. J. Maher, D. W. Janes, C. J. Ellison, and C. G. Willson, Block copolymer lithography, Macromolecules 47, 2 (2013).
- [9] J. Y. Cheng, C. A. Ross, E. L. Thomas, H. I. Smith, and G. J. Vancso, Fabrication of nanostructures with long-range order using block copolymer lithography, Appl. Phys. Lett. 81, 3657 (2002).
- [10] P. Maji and K. Naskar, Styrenic block copolymer-based thermoplastic elastomers in smart applications: Advances in synthesis, microstructure, and structure-property relationships—A review, J. Appl. Polym. Sci. 139, 5 (2022).
- [11] F. S. Bates, M. A. Hillmyer, T. P. Lodge, C. M. Bates, K. T. Delaney, and G. H. Fredrickson, Multiblock polymers: Panacea or pandora's box? Science 336, 434 (2012).
- [12] C. Zhang, D. L. Vigil, D. Sun, M. W. Bates, T. Loman, E. A. Murphy, S. M. Barbon, J. A. Song, B. Yu, G. H. Fredrickson et al., Emergence of hexagonally close-packed spheres in

- linear block copolymer melts, J. Am. Chem. Soc. **143**, 14106 (2021).
- [13] H. Feng, M. Dolejsi, N. Zhu, S. Yim, W. Loo, P. Ma, C. Zhou, G. S. W. Craig, W. Chen, L. Wan *et al.*, Optimized design of block copolymers with covarying properties for nanolithography, Nat. Mater. 21, 1426 (2022).
- [14] J. J. de Pablo, N. E. Jackson, M. A. Webb, L. Q. Chen, J. E. Moore, D. Morgan, R. Jacobs, T. Pollock, D. G. Schlom, E. S. Toberer *et al.*, New frontiers for the materials genome initiative, npj Comput. Mater. 5, 41 (2019).
- [15] Y. Liu, C. Niu, Z. Wang, Y. Gan, Y. Zhu, S. Sun, and T. Shen, Machine learning in materials genome initiative: A review, J. Mater. Sci. Technol. 57, 113 (2020).
- [16] M. L. Green, C. L. Choi, J. R. Hattrick-Simpers, A. M. Joshi, I. Takeuchi, S. C. Barron, E. Campo, T. Chiang, S. Empedocles, J. M. Gregoire *et al.*, Fulfilling the promise of the materials genome initiative with high-throughput experimental methodologies, Appl. Phys. Rev. 4, 011105 (2017).
- [17] T. H. Epps, E. W. Cochran, T. S. Bailey, R. S. Waletzko, C. M. Hardy, and F. S. Bates, Ordered network phases in linear poly(isoprene-b-styrene-b-ethylene oxide) triblock copolymers, Macromolecules 37, 8325 (2004).
- [18] A. K. Khandpur, S. Förster, F. S. Bates, I. W. Hamley, A. J. Ryan, W. Bras, K. Almdal, and K. Mortensen, Polyisoprenepolystyrene diblock copolymer phase diagram near the orderdisorder transition, Macromolecules 28, 8796 (1995).
- [19] D. A. Davidock, M. A. Hillmyer, and T. P. Lodge, Mapping large regions of diblock copolymer phase space by selective chemical modification, Macromolecules 37, 397 (2004).
- [20] Y. Ren, T. P. Lodge, and M. A. Hillmyer, A new class of fluorinated polymers by a mild, selective, and quantitative fluorination, J. Am. Chem. Soc. **120**, 6830 (1998).
- [21] Y. Ren, T. P. Lodge, and M. A. Hillmyer, Synthesis, characterization, and interaction strengths of difluorocarbene-modified polystyrene-polyisoprene block copolymers, Macromolecules **33**, 866 (2000).
- [22] A. Jayaraman and H.-A. Klok, ACS polymers Au's grand challenges in polymer science, ACS Polym. Au 3, 1 (2023).
- [23] C. Zhang, M. W. Bates, Z. Geng, A. E. Levi, D. Vigil, S. M. Barbon, T. Loman, K. T. Delaney, G. H. Fredrickson, C. M. Bates *et al.*, Rapid generation of block copolymer libraries using

- automated chromatographic separation, J. Am. Chem. Soc. 142, 9843 (2020).
- [24] X. Shi, M. Liu, L. Li, J. Zhang, H. Li, Z. Huang, W. Zhang, Z. Zhang, N. Zhou, and X. Zhu, Efficient synthesis of discrete oligo(fluorenediacetylene)s toward chain-length-dependent optical and structural properties, Polym. Chem. 12, 2598 (2021).
- [25] N. D. Ogbonna, M. Dearman, C. Cho, B. Bharti, A. J. Peters, and J. Lawrence, Topologically precise and discrete bottlebrush polymers: Synthesis, characterization, and structure-property relationships, JACS Au 2, 898 (2022).
- [26] M. Romio, B. Grob, L. Trachsel, A. Mattarei, G. Morgese, S. N. Ramakrishna, F. Niccolai, E. Guazzelli, C. Paradisi, E. Martinelli *et al.*, Dispersity within brushes plays a major role in determining their interfacial properties: The case of oligoxazoline-based graft polymers, J. Am. Chem. Soc. 143, 19067 (2021).
- [27] J. M. Ren, J. Lawrence, A. S. Knight, A. Abdilla, R. B. Zerdan, A. E. Levi, B. Oschmann, W. R. Gutekunst, S. H. Lee, Y. Li et al., Controlled formation and binding selectivity of discrete oligo(methyl methacrylate) stereocomplexes, J. Am. Chem. Soc. 140, 1945 (2018).
- [28] B. Oschmann, J. Lawrence, M. W. Schulze, J. M. Ren, A. Anastasaki, Y. Luo, M. D. Nothling, C. W. Pester, K. T. Delaney, L. A. Connal *et al.*, Effects of tailored dispersity on the self-assembly of dimethylsiloxane-methyl methacrylate block co-oligomers, ACS Macro Lett. 6, 668 (2017).
- [29] C. Zhang, D. S. Kim, J. Lawrence, C. J. Hawker, and A. K. Whittaker, Elucidating the impact of molecular structure on the <sup>19</sup>F NMR dynamics and MRI performance of fluorinated oligomers, ACS Macro Lett. 7, 921 (2018).
- [30] Y. Kim, H. Park, A. Abdilla, H. Yun, J. Han, G. E. Stein, C. J. Hawker, and B. J. Kim, Chain-length-dependent self-assembly behaviors of discrete conjugated oligo(3-hexylthiophene), Chem. Mater. 32, 3597 (2020).
- [31] J. J. Haven, J. A. De Neve, and T. Junkers, Versatile approach for the synthesis of sequence-defined monodisperse 18- and 20-mer oligoacrylates, ACS Macro Lett. 6, 743 (2017).
- [32] N. S. Vail, C. Stubbs, C. I. Biggs, and M. I. Gibson, Ultralow dispersity poly(vinyl alcohol) reveals significant dispersity effects on ice recrystallization inhibition activity, ACS Macro Lett. 6, 1001 (2017).
- [33] A. Das, K. Petkau-Milroy, G. Klerks, B. Van Genabeek, R. P. M. Lafleur, A. R. A. Palmans, and E. W. Meijer, Consequences of dispersity on the self-assembly of ABA-type amphiphilic block co-oligomers, ACS Macro Lett. 7, 546 (2018).
- [34] E. A. Murphy, Y.-Q. Chen, K. Albanese, J. R. Blankenship, A. Abdilla, M. W. Bates, C. Zhang, C. M. Bates, and C. J. Hawker, Efficient creation and morphological analysis of ABC triblock terpolymer libraries, Macromolecules 55, 8875 (2022).
- [35] J. De Neve, J. J. Haven, S. Harrisson, and T. Junkers, Deconstructing oligomer distributions: Discrete species and artificial distributions, Angew. Chemie **131**, 14007 (2019).
- [36] J. Chen, A. Rizvi, J. P. Patterson, and C. J. Hawker, Discrete libraries of amphiphilic poly(ethylene glycol) graft copolymers: Synthesis, assembly, and bioactivity, J. Am. Chem. Soc. 144, 19466 (2022).
- [37] J. Lawrence, S. H. Lee, A. Abdilla, M. D. Nothling, J. M. Ren, A. S. Knight, C. Fleischmann, Y. Li, A. S. Abrams, B. V. K. J. Schmidt *et al.*, A versatile and scalable strategy to discrete oligomers, J. Am. Chem. Soc. 138, 6306 (2016).

- [38] J. Lawrence, E. Goto, J. M. Ren, B. McDearmon, D. S. Kim, Y. Ochiai, P. G. Clark, D. Laitar, T. Higashihara, and C. J. Hawker, A versatile and efficient strategy to discrete conjugated oligomers, J. Am. Chem. Soc. 139, 13735 (2017).
- [39] J. J. Haven, J. De Neve, A. Castro Villavicencio, and T. Junkers, Elucidation of the properties of discrete oligo(meth)acrylates, Polym. Chem. 10, 6540 (2019).
- [40] J. J. Haven and T. Junkers, Quasi-monodisperse polymer libraries: Via flash column chromatography: Correlating dispersity with glass transition, Polym. Chem. 10, 679 (2019).
- [41] J. E. Báez, K. J. Shea, P. R. Dennison, A. Obregón-Herrera, and J. Bonilla-Cruz, Monodisperse oligo( $\delta$ -valerolactones) and oligo( $\epsilon$ -caprolactones) with docosyl ( $C_{22}$ ) end-groups, Polym. Chem. **11**, 4228 (2020).
- [42] Y. Hoshino, S. Taniguchi, H. Takimoto, S. Akashi, S. Katakami, Y. Yonamine, and Y. Miura, Homogeneous oligomeric ligands prepared via radical polymerization that recognize and neutralize a target peptide, Angew. Chem., Int. Ed. 59, 679 (2020).
- [43] L. Maes, D. Massana Roqeuro, L. M. Pitet, P. Adriaensens, and T. Junkers, Sequence-defined nucleobase containing oligomers: Via reversible addition-fragmentation chain transfer single monomer addition, Polym. Chem. 11, 2027 (2020).
- [44] See Supplemental Material at http://link.aps.org/supplemental/ 10.1103/PhysRevMaterials.8.015602 for reagent information, experimental procedures, <sup>1</sup>H NMR spectroscopy data, sizeexclusion chromatograms, DSC thermograms, automated chromatography method, and small angle x-ray scattering patterns.
- [45] E. H. Discekici, A. Anastasaki, R. Kaminker, J. Willenbacher, N. P. Truong, C. Fleischmann, B. Oschmann, D. J. Lunn, J. Read De Alaniz, T. P. Davis *et al.*, Light-mediated atom transfer radical polymerization of semi-fluorinated (meth)acrylates: Facile access to functional materials, J. Am. Chem. Soc. 139, 5939 (2017).
- [46] S. Jo, S. Jeon, T. Jun, C. Park, and D. Y. Ryu, Fluorine-containing styrenic block copolymers toward high  $\chi$  and perpendicular lamellae in thin films, Macromolecules **51**, 7152 (2018).
- [47] C. Cummins, D. Mantione, F. Cruciani, G. Pino, N. Demazy, Y. Shi, G. Portale, G. Hadziioannou, and G. Fleury, Rapid self-assembly and sequential infiltration synthesis of high χ fluorine-containing block copolymers, Macromolecules 53, 6246 (2020).
- [48] C. Wang, X. Li, and H. Deng, Synthesis of a fluoromethacrylate hydroxystyrene block copolymer capable of rapidly forming sub-5 nm domains at low temperatures, ACS Macro Lett. **8**, 368 (2019).
- [49] R. Maeda, T. Hayakawa, and C. K. Ober, Dual mode patterning of fluorine-containing block copolymers through combined top-down and bottom-up lithograph, Chem. Mater. 24, 1454 (2012).
- [50] M. W. Matsen, Phase behavior of block copolymer/homopolymer blends, Macromolecules 28, 5765 (2002).
- [51] B. Zhang, S. Xie, T. P. Lodge, and F. S. Bates, Phase behavior of diblock copolymer-homopolymer ternary blends with a compositionally asymmetric diblock copolymer, Macromolecules 54, 460 (2021).
- [52] J. Xie and A.-C. Shi, Formation of complex spherical packing phases in diblock copolymer/homopolymer blends, Giant 5, 100043 (2021).
- [53] B. Yu, R. Li, and R. A. Segalman, Tuning the double gyroid phase window in block copolymers via polymer chain

- conformation near the interface, Macromolecules **54**, 5388 (2021).
- [54] M. Liu, Y. Qiang, W. Li, F. Qiu, and A.-C. Shi, Stabilizing the Frank-Kasper phases via binary blends of AB diblock copolymers, ACS Macro Lett. 5, 1167 (2016).
- [55] E. W. Cochran, C. J. Garcia-Cervera, and G. H. Fredrickson, Stability of the gyroid phase in diblock copolymers at strong segregation, Macromolecules 39, 2449 (2006).
- [56] S. Lee, M. Bluemle, and F. S. Bates, Discovery of a Frank-Kasper  $\sigma$  phase in sphere-forming block copolymer melts, Science **330**, 349 (2010).
- [57] M. W. Bates, J. Lequieu, S. M. Barbon, R. M. Lewis, K. T. Delaney, A. Anastasaki, C. J. Hawker, G. H. Fredrickson, and C. M. Bates, Stability of the A15 phase in diblock copolymer melts, Proc. Natl. Acad. Sci. USA 116, 13194 (2019).
- [58] A. B. Chang and F. S. Bates, Impact of architectural asymmetry on Frank-Kasper phase formation in block polymer melts, ACS Nano 14, 11463 (2020).
- [59] M. W. Bates, S. M. Barbon, A. E. Levi, R. M. Lewis, H. K. Beech, K. M. Vonk, C. Zhang, G. H. Fredrickson, C. J. Hawker, and C. M. Bates, Synthesis and self-assembly of AB<sub>n</sub> miktoarm star polymers, ACS Macro Lett. **9**, 396 (2020).
- [60] Y. Sun, R. Tan, Z. Ma, Z. Gan, G. Li, D. Zhou, Y. Shao, W.-B. Zhang, R. Zhang, and X.-H. Dong, Discrete block copolymers with diverse architectures: Resolving complex spherical phases with one monomer resolution, ACS Cent. Sci. 6, 1386 (2020).
- [61] Z. Ma, R. Tan, Z. Gan, D. Zhou, Y. Yang, W. Zhang, and X.-H. Dong, Modulation of the complex spherical packings through rationally doping a discrete homopolymer into a discrete block copolymer: A quantitative study, Macromolecules 55, 4331 (2022).
- [62] A. J. Mueller, A. P. Lindsay, A. Jayaraman, T. P. Lodge, M. K. Mahanthappa, and F. S. Bates, Emergence of a C15 laves phase in diblock polymer/homopolymer blends, ACS Macro Lett. 9, 576 (2020).
- [63] N. A. Lynd and M. A. Hillmyer, Influence of polydispersity on the self-assembly of diblock copolymers, Macromolecules 38, 8803 (2005).
- [64] K. D. Dorfman, Frank-Kasper phases in block polymers, Macromolecules 54, 10251 (2021).
- [65] G. K. Cheong, F. S. Bates, and K. D. Dorfman, Symmetry breaking in particle-forming diblock polymer/homopolymer blends, Proc. Natl. Acad. Sci. USA 117, 16764 (2020).

- [66] D. Cai, J. Li, Z. Ma, Z. Gan, Y. Shao, Q. Xing, R. Tan, and X.-H.Dong, Effect of molecular architecture and symmetry on self-assembly: A quantitative revisit using discrete ABA triblock copolymers, ACS Macro Lett. 11, 555 (2022).
- [67] B. A. G. Lamers, B. Van Genabeek, J. Hennissen, B. F. M. De Waal, A. R. A. Palmans, and E. W. Meijer, Stereocomplexes of discrete, isotactic lactic acid oligomers conjugated with oligodimethylsiloxanes, Macromolecules 52, 1200 (2019).
- [68] B. Van Genabeek, B. F. M. De Waal, M. M. J. Gosens, L. M. Pitet, A. R. A. Palmans, and E. W. Meijer, Synthesis and self-assembly of discrete dimethylsiloxane-lactic acid diblock co-oligomers: The dononacontamer and its shorter homologues, J. Am. Chem. Soc. 138, 4210 (2016).
- [69] D. T. Gentekos, J. Jia, E. S. Tirado, K. P. Barteau, D.-M. Smilgies, R. A. DiStasio, Jr., and B. P. Fors, Exploiting molecular weight distribution shape to tune domain spacing in block copolymer thin films, J. Am. Chem. Soc. 140, 4639 (2018).
- [70] A. K. Schmitt and M. K. Mahanthappa, Order and disorder in high χ/low *N*, broad dispersity ABA triblock polymers, Macromolecules **50**, 6779 (2017).
- [71] M. W. Matsen, Effect of large degrees of polydispersity on strongly segregated block copolymers, Eur. Phys. J. E 21, 199 (2006).
- [72] C. Sinturel, F. S. Bates, and M. A. Hillmyer, High χ-low N block polymers: How far can we go? ACS Macro Lett. 4, 1044 (2015).
- [73] T. Seshimo, R. Maeda, R. Odashima, Y. Takenaka, D. Kawana, K. Ohmori, and T. Hayakawa, Perpendicularly oriented sub-10-nm block copolymer lamellae by atmospheric thermal annealing for one minute, Sci. Rep. 6, 19481 (2016).
- [74] J. Lequieu, T. Quah, K. T. Delaney, and G. H. Fredrickson, Complete photonic band gaps with nonfrustrated ABC bottlebrush block polymers, ACS Macro Lett. 9, 1074 (2020).
- [75] B. B. Patel, D. J. Walsh, D. H. Kim, J. Kwok, B. Lee, D. Guironnet, and Y. Diao, Tunable structural color of bottlebrush block copolymers through direct-write 3D printing from solution, Sci. Adv. 6, eaaz7202 (2020).
- [76] E. Murphy, S. Skala, D. Kottage, P. Kohl, Y. Li, C. Zhang, C. Hawker, and C. Bates, Accelerated discovery and mapping of block copolymer phase diagrams [Data set]. Dryad (2023), https://datadryad.org/stash/dataset/doi:10.5061/dryad.41ns1rnm6.
- [77] www.mrfn.org.